







Research Article

Large Deformation Mechanics of Gob-Side Roadway and Its Controlling Methods in Deep Coal Mining: A Case Study

Jianwei Zheng ^{1,2,3} Wenjun Ju ^{1,2,3} Xiaodong Sun ^{1,2,3} Zhongwei Li ^{1,2,3}
Shuai Wang ⁴ and Biao Liu ⁵

¹Beijing Mining Research Institute, China Coal Research Institute, Beijing 100013, China

²CCTEG Coal Mining Research Institute, Beijing 100013, China

³Coal Mining & Designing Department, Tiandi Science & Technology Co., Ltd., Beijing 100013, China

⁴China Coal Technology and Engineering Group Shenyang Research Institute, Fushun 113122, China

⁵Tongchuan Mining, Shaanxi Coal and Chemical Industry Group Co., Ltd., Tongchuan, Shaanxi 727101, China

Correspondence should be addressed to Jianwei Zheng; zhengjanvy@163.com

Received 24 June 2020; Revised 21 November 2020; Accepted 7 December 2020; Published 19 December 2020

Academic Editor: Francesco Colangelo

Copyright © 2020 Jianwei Zheng et al. This is an open access article distributed under the Creative Commons Attribution License, which permits unrestricted use, distribution, and reproduction in any medium, provided the original work is properly cited.

Maintaining surrounding rock mass stability of roadways is essential to the safety of deep coal mining. In this study, the No. 2-2092 roadway of the No. 2-209 mining face in Ganhe coal was taken as the target roadway for field analysis. The selected region can be considered a typical area with dominating geological tectonic stress, based on the geological survey and in situ stress results. A mechanical model of roadway overburdens was developed to analyse the large deformation and stress field distribution. It is found that the large deformation is caused by the combined superposed stress field including laterally transferred stress formed in structures at overlying strata, mining-induced advanced abutment pressure, and the regional in situ stress. Thus, a Two-Direction Hydrofracturing Technique (TDHT) was proposed to reduce the pressure of the No. 2-2092 roadway by altering the roof structure in the influenced zones. Compared with the original roadway without fracturing, it is found that the roof to floor convergence has dropped by nearly 47% after fracturing; the displacement of sidewalls has reduced by almost 31%, demonstrating the effectiveness of the proposed method in pressure relief. Results from this study can provide guidance on controlling the large deformation of roadways in deep underground mines.

1. Introduction

The statistics of Statistical Review of World Energy indicated that, in the global primary energy structure in 2018, coal accounted for 28% of total energy, where coal output reached about 3.68 billion tons in China [1], contributing to 59% of China's primary energy consumption (2018) [2, 3]. As estimated by International Energy Agency, coal will account for 22% in the global energy structure for up to 2040, and China will still be the largest energy consumer in the globe with its coal output occupying 50% of global demand [4]. With nearly 70 years of intensive coal mining and continuously growing mining depth in China (the mining deepening rate is over 10–25 m/year across China), deep underground mining is faced with a harsh mining

environment featuring “existence state with high in situ stress, high operating ambient temperature, highly confined water condition, high-gas and high-impact mine pressure tendency, strong mining-induced stress disturbance, and engineering disturbance from adjacent roadway groups” [5–8]. The main factors for causing the harsh mining environment include the following: (1) more exasperated geological conditions that cannot be elaborately proved; (2) complex surrounding rock stress environment under multifield disturbance; and (3) unstable caving of the overlying strata structure formed in the mined area. The number of deep mines is still increasing, and large deformation disaster is becoming even more violent in the roadway during the deep mining process [9–11], especially for the gob-side roadways [12]. Production and transportation of coal

mining can be easily influenced by large deformation that occurred in roadway surrounding rock. In addition, the normalized “floor heaving” and “side expansion” workload will be abruptly increased, along with the increase of labour intensity. When the working face is located in a geologic body with burst tendency, it will even cause fierce dynamic instability-induced disasters, which severely threaten the safety of underground workers [13–16]. Therefore, it is of great importance to unveil the mechanism of large deformation of surrounding rocks in deep gob-side roadways and provide corresponding control measures.

In the classical roadway mechanical analysis, elastic solution of the round hole is often used to analyse the boundary stress conditions [17]. According to the “Theory of Axial Variation” proposed by Yu [18], the deformation in the roadway is directly related to the ratio of the horizontal stress to vertical stress. Li et al. [19] established a mechanical model of roadway that occurred in nonuniform stress conditions based on the unified strength theory and derived the theoretical range of the plastic zone. Maleki and Mousivand [20] conducted the elastic-plastic analysis of roadway surrounding rock mass. Sharan [21] used the Hoek–Brown criterion to analyse the stress and displacement distribution of surrounding rock in a circular roadway. Hou and Yang [22] developed a physical model of the roadway to obtain the real-time surface displacement with DIC (Digital Image Correlation). Zhu et al. [23] provided the elastoplastic analysis of roadway using the statistical damage constitutive model and derived the stress distribution of roadway. Zheng et al. [24] analysed the range of roadway elastic-plastic zone under three-directional stresses. Yuan et al. [25] deduced the boundary equations of the roadway and discussed the main factors related to roadway stability. Xue et al. [26] obtained the stress-strain solutions of roadway considering both creep deformation and strain softening.

Considering the large deformation occurring in the gob-side roadway, some scholars believed that the movement of the overlying strata can be reduced or relieved by filling the goaf to maintain the stability of the gob-side roadway [27], and related studies were conducted for filling materials, filling processes, and filling effects. However, the application of the approach was limited due to the high cost. Previous studies suggested that the large deformation of a roadway can be resisted by strengthening the roadway support intensity [28–32], for example, selecting higher-quality bolt and cable, adjusting support parameters, and using steel band and metal net as auxiliary members [33–35]. Later, some scholars argued that these supporting approaches have only limited control over the actual large deformation of roadways, and, under most circumstances, the large deformation is governed by the self-bearing capacity of surrounding rocks [36, 37]. Theories such as “self-stabilization balance ring,” “equivalent cross section,” and “invisible load-carrying arch” have been proposed to reduce the large deformation through the synergistic effect of manual support and bearing capacity of surrounding rocks [38–40]. When the geological conditions of roadways become more complicated, the stress grade may grow higher. Some scholars

proposed maintaining roadway stability through pressure relief or stress transfer. Han et al. [41] established a masonry beam model of spatial gob-side roadway structure under the hard roof condition and proposed the detonation-assisted roof cutting technique. Ma et al. [42] simulated the mining process with retained gob-side entry by FLAC3D and found that the roadway deformation could be effectively reduced by strengthening the support intensity and by roof cutting. Huang et al. [43] found that using hydrofracturing in the gob-side roadway, the overhung roof in the adjacent goaf could be cut off, which may reduce the large deformation of the roadway. Kang et al. [44] found that the hydrofracturing technique could lower the stress concentration in the roadway by generating new cracks.

Many scholars have investigated the instability mechanism of deep mining roadways and stability control techniques for surrounding rocks [45–54]. However, the research on the large deformation controlling method of gob-side roadway occurring in the deep coal mine is still needed, including the mechanical model of the gob-side roadway and the methods to deal with this unfavourable displacement. Therefore, based on the 2-2092 roadway (rail haulage roadway) in the Ganhe Coal mine, geological survey and in situ stress measurement were combined to study the overall mechanical characteristics in the mining region. A mechanical model of the 2-2092 roadway was developed to analyse the dynamic evolution of the spatial structure of surrounding rocks in the mining roadway. The Two-Direction Hydrofracturing Technique (TDHT) was proposed to control large deformation disasters according to the stress features of the deep gob-side roadway, and satisfactory results were achieved. This could provide useful knowledge for controlling large deformation in the deep gob-side roadway and for safe advancement of the working face under similar geological conditions.

2. Site Details

2.1. Mining Background. The Ganhe coal mine is located in the north of Hongdong County, Shanxi Province, with a total minefield area of 35.56 km² in the NE-SW stripped distribution. The designed production capacity is 2.4 Mt/year. The 2-209 working face mainly mines the 2# coal seam in the Permian Tongshanxi Formation. The thickness of the coal seam is about 3.69 m, and the overall dip angle is 4°. The target roadway is a rail haulage roadway (2-2092 roadway) of the 2-209 working face that is currently under mining, and the 2-209 working face is 183.00 m in length with an average mining depth of 500.00 m, where 40–100.00 m of the loess layer and about 394.00 m of bedrock layer are overlaid. Both the 2-2091 roadway (belt conveying roadway) and 2-2092 roadway (rail haulage roadway) are coal roadways. The 2-2092 roadway is close to the 2–100 working face goaf and the width of coal pillars between the two working faces is 25.00 m. The spatial relationship between the 2-209 working face and adjacent working face is shown in Figure 1.

The immediate roof of the 2-209 working face mainly consists of grey semihard siltstone with thin siderite mudstone, and its thickness is 1.59 m. The upper part contains

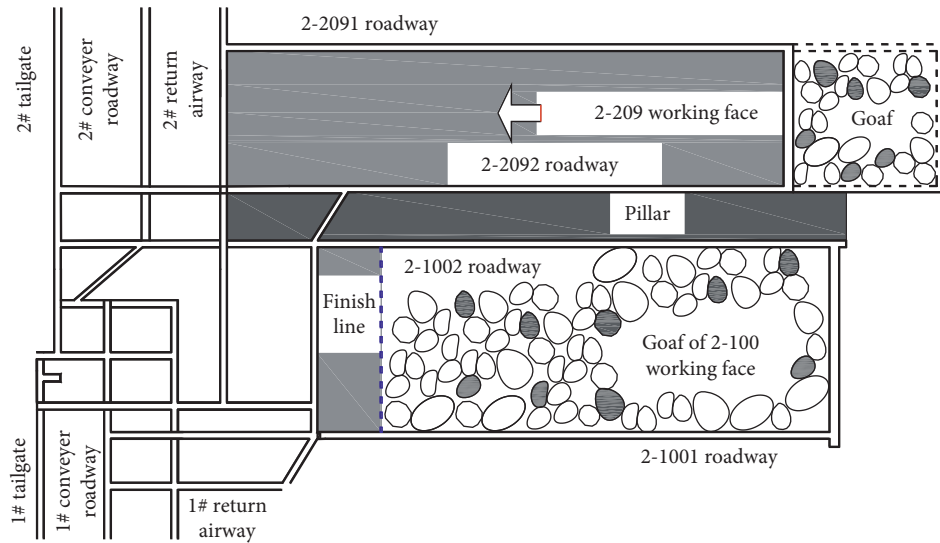


FIGURE 1: Spatial relationship between 2-209 working face and adjacent working face.

dark grey mudstone with 4.20 m in thickness. The immediate floor is lentoid stratified silt with 1.61 m in thickness. Through in situ strength test of roadway roof and sidewalls using the WQCZ-56 surrounding rock strength test system, the measured average strata strength was 53.36–57.32 MPa in the range of 0.00–5.00 m above the roof, and 37.45–38.20 MPa within 5.00–10.00 m above the roof; the average strength value was 14.54 MPa for the 2# coal seam.

2.2. Geological Details. Located in the Huoxi coalfield, the Ganhe coal mine is in the north of Hongdong area of Shanxi transition block (level III) on the north China plate (level II), wherein its east and west are the Huoshan normal fault and Luoyunshan normal fault, respectively, and in the south and north sides are the Xiazhangduan normal fault and Xia-tuanbai normal fault, respectively. Various vertically and longitudinally distributed structures, as well as shear structures, are presented, where the Shilin fault is the largest east-west structure with intense activities, and the Shang-tuanbai fault is mainly in the compressive structural plane. Within the Ganhe coal mine and its adjacent region, there are 3 folds, 15 faults (with distances greater than 5.00 m), and 6 collapse columns. The internal geological structures are complex and staggered, which affects in situ stress distribution in the coalfield. The geological structural information of the Ganhe coal mine is shown in Figure 2.

2.3. Excavation Problems. The on-site observational data showed that the roadway section geometry and supporting effects were effective during the excavation period of 2-2092 roadway, and no obvious roadway deformation was observed. After the 2-209 working face advanced into the influenced scope of the 2-100 working face goaf, severe deformation failure appeared in the area of mining-induced advanced abutment pressure of the 2-2092 roadway. The general feature is summarized as follows: in the advanced 150 m region, the hard layer of the floor experienced

cracking with an obvious floor heaving trend. In the advanced 60 m region, deformation failure was aggravated in the 2-2092 roadway, the floor was fiercely heaved, the metal net was broken appearing on the roof, the roadway height declined from 3.6 m to 2.5 m, and the convergence of roof to floor reached as high as 1.1 m. The two sidewalls went through severe deformation failure simultaneously. The roadway width reduced from 4.8 m to 3.5 m and the displacement of the two sidewalls reached 1.3 m; the reduction rate of the effective spatial section reached 50%. Four rows of single hydraulic props and π -shaped beams were arranged within the area of mining-induced advanced abutment pressure in the 2-2092 roadway to reinforce the advanced support, but the roadway deformation was still serious as shown in Figure 3.

To decrease the side effect of large deformation in the 2-2092 roadway, roadway repairing methods, including floor heaving and sides clearing, were adopted. However, this governance mode is a typical passive remedial treatment measure with 3 following serious problems in the actual operation process: (1) governance effect is not ideal with large labour intensity and it takes a long time; (2) annual governance cost is high; and (3) the adopted measures may be temporarily effective and the hidden danger of mine pressure disaster is still existing, which not only influenced working efficiency of coal mine workers but also seriously impacted normal life of mine workers. Therefore, it is necessary to analyse the large deformation mechanism of the gob-side roadway for more pertinent and practical measures to solve this problem.

3. Superposed Stress Analysis of Surrounding Rocks in Mining Roadway

Through a long-term observation of 2-2092 mining roadway, the deformation of the target roadway abruptly increased during the mining period when entering the area of mining-induced advanced abutment pressure. According to

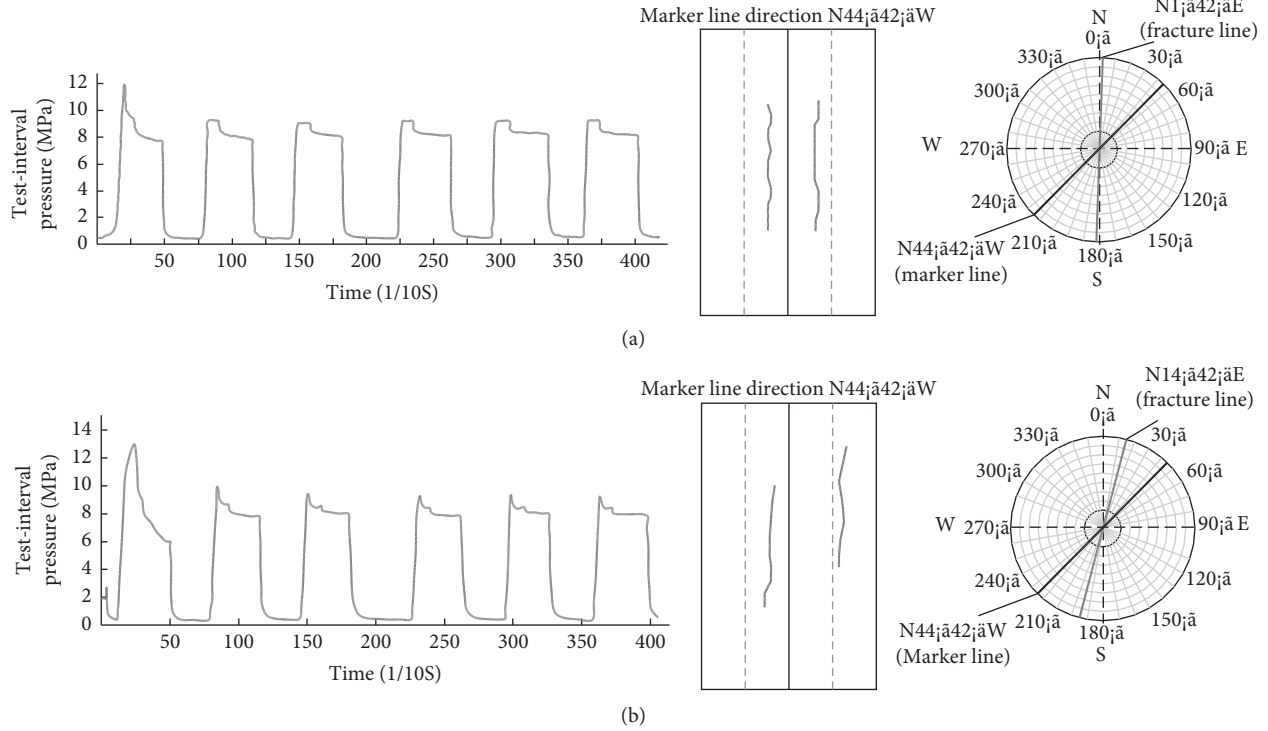


FIGURE 4: Pressure-time curve and fracturing direction obtained at (a) 1# measuring point and (b) 2# measuring point.

medium-stress areas. The measurement results at the two measuring points both indicated that the maximum horizontal principal stress was greater than the vertical principal stress, as confirmed by the obvious directional deformation of the roadway that demonstrated a typical $\sigma_H > \sigma_V > \sigma_h$ stress field. This area was mainly a tectonic stress field, where the maximum principal stress played a dominant role and the direction was approximately in the N-S direction.

3.2. Lateral Stress Field Analysis of the Mining Roadway. One side of the 2-2092 roadway was close to the goaf of the 2-100 working face, and the width of coal pillars was 25.00 m. During the 2-2092 roadway excavation period, the coal pillar-side deformation was greater than coal seam-side deformation in the excavation process, but the overall roadway deformation was kept at a low level. It could be indicated from the analysis that the periodic weighting imposed on coal pillars, generated by 2-100 working face advancing, which reduced the overall strength of coal pillars and enlarged injury degree of coal pillars (internal cracks were developed and ran through each other), weakened their permanent bearing capacity, but the coal pillars were in a favourable bearing structural system on the whole, thus meeting the requirement for maintaining roadway safety. The roof went through periodic fracturing collapse in the mining process of the 2-100 working face, a certain spatial structure was formed at overlying strata, coal pillars were under a high stress state, and the coal pillar-side deformation was larger than the coal seam-side deformation in the excavation process of the 2-2092 roadway.

The stress imposed on coal pillars without mining effect was simplified, and it could be considered that the external load on coal pillars mainly consisted of two parts as shown in formula (1), where one part is the weight (vertical stress, σ_{p0}) of the overlying strata at the coal pillar side and the other part is the increment ($\sum_1^n f_p(x)$) internal stress of coal pillars transferred by the spatial structure, which is formed at the upper strata in the goaf of the 2-100 working face. As the 2-100 working face was already mined, the structures formed within the scope of the 2-100 working face goaf are stable. It is shown that a cantilever beam-like spatial 3D structure is formed nearby the coal pillars, the mechanical model of coal pillars is shown in Figure 5, and the stress occurring in coal pillars is shown in formula (2): where $f_1(x)$, $f_2(x)$, and $f_n(x)$ are internal stress increment of coal pillars caused by an external load, which is transferred from the cantilever beam structures at the first mining stratum, second stratum, and n^{th} stratum (different strata) to coal pillars, respectively, MPa; γ_1 , γ_2 , and γ_n denote strata volume weights at different strata, N/m^3 ; h_1 , h_2 , and h_n are thickness values of rock blocks in the structures at different strata, m ; and l_{h1} , l_{h2} , and l_{hn} are lengths of cantilever-like rock blocks in the structures at different strata, m .

$$\sigma_p = \sigma_{p0} + \sum_1^n f_p(x) = lh_1\gamma_1 + lh_2\gamma_2 + \dots + lh_n\gamma_n + \sum_1^n f_p(x), \tag{1}$$

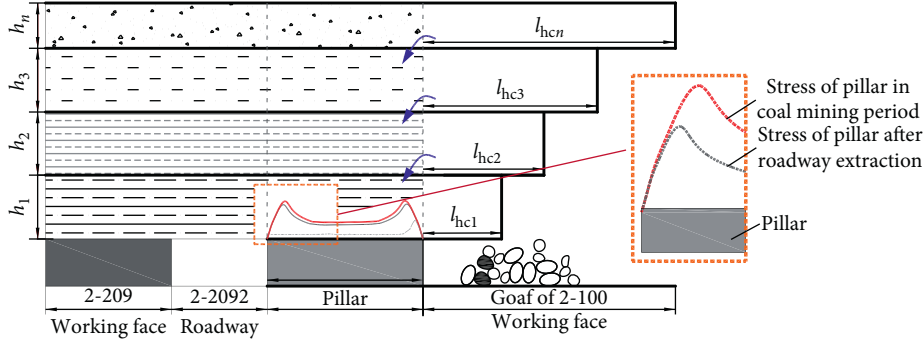


FIGURE 5: Mechanical model of the coal pillar side in 2-2092 roadway.

$$\sum_1^n f_p(x) = f_1(x) + f_2(x) + \dots + f_n(x) \quad (2)$$

$$= l_{h1}h_1\gamma_1 + l_{h2}h_2\gamma_2 + \dots + l_{hn}h_n\gamma_n$$

From equations (1) and (2), formula (3) can be obtained and the formula represents the internal stress (σ_p) when coal pillars are not disturbed by mining. Accordingly, the external load imposed on the coal pillar side is mainly a function of the overhanging length (l_h) of the rock beam above the coal seam. As the length of the cantilever beam at overlying strata in the goaf increases, the greater the internal stress value in coal pillars is, the greater the (σ_p) value will be:

$$\sigma_p = h_1\gamma_1(l + l_{h1}) + h_2\gamma_2(l + l_{h2}) + \dots + h_n\gamma_n(l + l_{hn}). \quad (3)$$

3.3. Analysis of Mining-Induced Advanced Abutment Pressure Field in the Mining Roadway. With the advancing of the working face, mining-induced advanced abutment pressure would be formed in the coal seam, as influenced by the stress redistribution. The mechanical characteristic of the coal seam within this influencing scope was analysed as follows: a “cantilever beam + hinged beam” spatial structure would be formed in the mining process at the overlying inferior strata on the working face. This structure acted at the front coal seam of the working face, so as to cause the increase of the mining-induced advanced abutment pressure (σ_c), which mainly consisted of two parts: the first part was the vertical stress (σ_{co}) at the overlying strata on the coal seam and the second part was the internal stress increment ($\sum_1^n f_c(x)$) of coal pillars caused by the external load transferred by the “cantilever beam + hinged beam” spatial structure, which was formed at the strata in the stope, as shown in formula (4). The stress state of the coal seam was simplified and it could be considered that the stress increment caused by mining was mainly a function of the overhanging length (l_a) of the rock beam above the coal seam, geometrical rotation parameters, angle (θ) of intermediate rock block (B), and force transfer coefficient (η) from the hinged structure formed by the rock beam at different strata to lower the coal seam, as shown in formula (5). The mining-induced mechanical model of structures at the overlying strata is shown in Figure 6:

$$\sigma_c = \sigma_{co} + \sum_1^n f_c(x) = Lh_1\gamma_1 + Lh_2\gamma_2 + \dots + Lh_n\gamma_n + \sum_1^n f_c(x), \quad (4)$$

$$\sum_1^n f_c(x) = f_1(x) + f_2(x) + \dots + f_n(x)$$

$$= \eta_1 \times [l_{a1}h_1\gamma_1 + \Phi_1(l_{b1}, h_1, \gamma_1, \theta_1)] + \eta_2 \times [l_{a2}h_2\gamma_2 + \Phi_2(l_{b2}, h_2, \gamma_2, \theta_2)] + \dots + \eta_n \times [l_{an}h_n\gamma_n + \Phi_n(l_{bn}, h_n, \gamma_n, \theta_n)]. \quad (5)$$

where $f_1(x)$, $f_2(x)$, and $f_n(x)$ are increment components of the internal stress of coal pillars caused by external load transferred by structures at the first mining stratum, second stratum, and n^{th} stratum, respectively, MPa; Φ_1 , Φ_2 , and Φ_n are the acting force function of intermediate rock blocks in structures at different strata, respectively; η_1 , η_2 , and η_n are stress transfer coefficients in structures at different strata; l_{a1} , l_{a2} , and l_{an} are lengths of cantilever rock blocks in structures at different strata, m ; l_{b1} , l_{b2} , and l_{bn} are lengths of intermediate rock masses in structures at different strata, m ; and θ_1 , θ_2 , and θ_n are rotation angles of intermediate rock blocks in structures at different strata, $^\circ$. Based on formulas (4) and (5), the mining-induced advanced abutment pressure occurring inside the coal seam is expressed as

$$\sigma_c = \sigma_{co} + \sum_1^n f_c(x) = Lh_1\gamma_1 + Lh_2\gamma_2 + \dots + Lh_n\gamma_n + \eta_1 \times [l_{a1}h_1\gamma_1 + \Phi_1(l_{b1}, h_1, \gamma_1, \theta_1)] + \eta_2 \times [l_{a2}h_2\gamma_2 + \Phi_2(l_{b2}, h_2, \gamma_2, \theta_2)] + \dots + \eta_n \times [l_{an}h_n\gamma_n + \Phi_n(l_{bn}, h_n, \gamma_n, \theta_n)]. \quad (6)$$

It could be found from formula (6) that, with the increase of overhanging length (l_a) of the rock beam above the coal seam, geometrical rotation parameters, angle (θ) of intermediate rock block (B), and stress transfer coefficient (η) of the hinged structure formed by rock beams at different

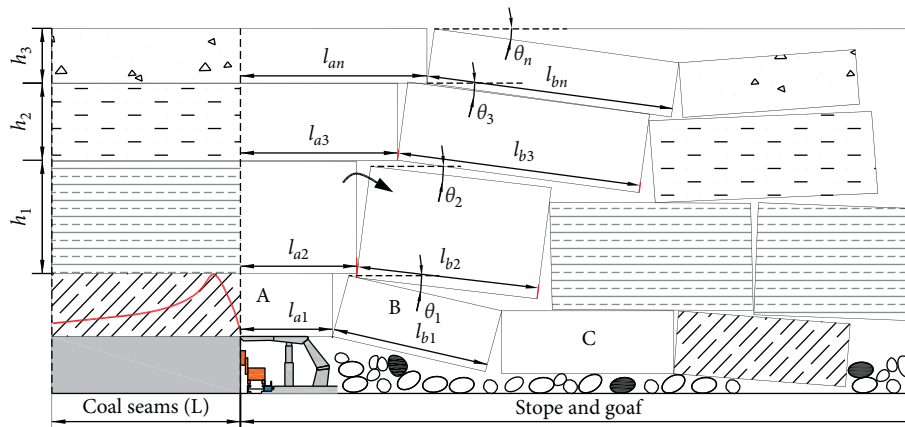


FIGURE 6: Mechanical model of mining-induced structures at the overlying strata.

strata, the stress increment caused by mining would gradually increase.

4. Two-Direction Hydrofracturing Technique and Performance Analysis

Based on the above analysis of the time and spatial effects of large deformation of the 2-2092 mining roadway, it is found that the deep geological tectonic stress, lateral transferred stress, and mining-induced advanced abutment pressure were the primary causes for stress increment of surrounding rocks in the 2-2092 roadway. The influencing scopes of the superposed stress are shown in Figure 7. Therefore, it is believed in this study that the spatial structure at the overlying strata in the 2-2092 roadway was changed through manual measures to realize roadway stress control, reducing the stress of roadway surrounding rocks and then lowering the large deformation degree of the roadway.

4.1. Two-Direction Hydrofracturing Technique. Based on the stress analysis of surrounding rocks in the 2-2092 roadway, the TDHT was applied within the 150.00 m advancing scope of the 2-209 working face. Hydrofracturing-induced fractures were set at specific positions so as to reduce the length of the stable cantilever occurring in the 2-100 working face goaf, which could lower the grade of lateral transferred stress. The spatial strata structure of the 2-209 working face goaf could be changed by applying the hydrofracturing technique, in order to lower the mining-induced stress grade transferred by the “cantilever + hinged” structure. Therefore, the proposed TDHT could simultaneously reduce lateral stress grade and mining-induced stress grade in the roadway, which can reach the goal of controlling the stress grade of the roadway surrounding rocks and lowering the roadway deformation. The TDHT parameter is determined by referring to relevant literature on hydraulic fracturing [55–58], considering regular hydraulic fracturing parameters of other working faces with similar mining conditions in the researched coalfield and basing on the thickness of roof strata, lithology, and strata characteristics of the 2-209 working face. The TDHT parameters are shown in Table 1

and the technical layout of the TDHT is shown in Figure 8. The design of the fracturing hole S' in the hydrofracturing scheme aimed at changing the integrity parallel to the roadway axis in the mining process of the working face. The continuity of structural planes or cracks on the hard roof was damaged and their strength was reduced at 150.00 m in front of the working face; thus, the roof could timely collapse according to the designed length. The design of the fracturing hole S aimed at laying structural planes or cracks on the advanced working face with two functions, including changing the cantilever length of the cantilever beam structure on the overhanging-side roof and changing the stress state of the overhanging-side cantilever. The cantilever beam was turned into a semi-imply supported beam to lower the stress concentration degree at the supporting position, and the roof collapse is more likely to take place. Fracturing holes S and S' jointly acted upon the hard roof and, meanwhile, the collapse form was changed from the advancing direction of the working face to the direction perpendicular to the roadway axis, which realizes the adjustment of stress environment of the gob-side roadway.

This TDHT mainly included hole sealing, high-pressure water fracturing, and pressure maintaining water injection procedures, and the main step was to push the hole packer to the designed position with columns connecting water injection pipes to implement the hole sealing procedure. Fracturing was performed using the retrusive fracturing method, that is, fracturing outward from bottom of drill hole successively. It is necessary to observe the drill hole and monitor the pressure gauge and detect whether the hole packer could maintain the pressure. If water flowed out of the drill hole or pressure dropped obviously, the hole sealing failed, and then the junction of the hole packer should be checked to ensure its normal operation. The fracturing area was continuously pressurized until cracking, and at the same time, the pressure would suddenly drop. Pressure maintaining water injection led to continuous crack expansion together with the generation of new cracks, and the pressure maintaining water injection fracturing time was determined according to on-site fracturing conditions. If water effused or burst out of the roadway roof, coal seam, or drill hole, fracturing should be immediately stopped.

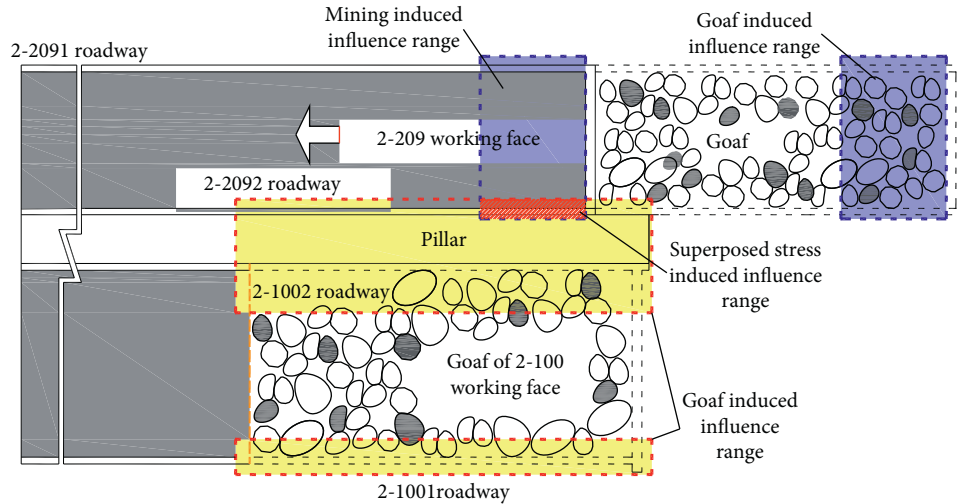


FIGURE 7: Influencing scope of superposed stress.

TABLE 1: Two-direction hydrofracturing parameters.

No.	Length of hole (m)	Diameter of hole (mm)	Elevation angle of hole (°)	Included angle between hole and roadway (°)	Hole spacing (m)	Fracturing time (min)	Fracturing interval (m)	Single-hole fracturing times
S	40.5	50	50	90	16	30	2-3	10-13
S'	40.5	50	50	3-5	8	30	2-3	10-13

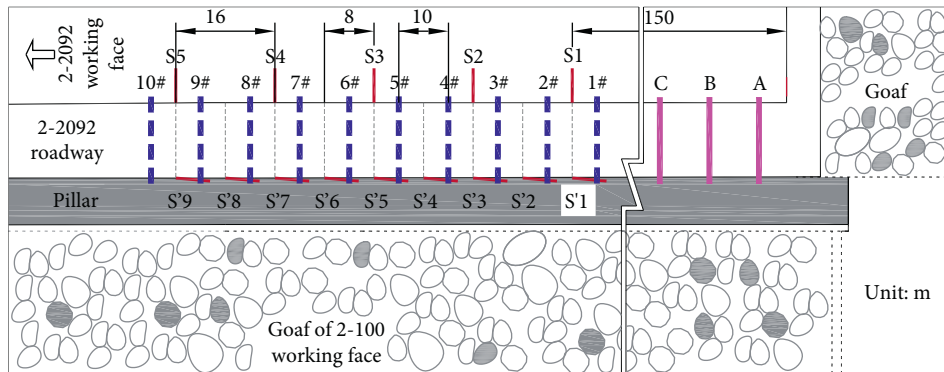


FIGURE 8: Arrangement of the DHT and the associated monitoring.

4.2. *Effect Analysis.* In order to verify the effect of TDHT, three convergence monitoring stations (termed A, B, and C) were set outside the fracturing scope, and another 10 convergence monitoring stations (numbered 1#–10#) were arranged within the fracturing scope with an interval of 10.00 m. The roof to floor convergence and displacement of two sidewalls were monitored in both the fracturing area and nonfracturing area of the 2-2092 roadway. The results of the area without applying the TDHT are shown in Figures 9(a) and 9(b). It was found that the roadway roof to floor convergence decreased with the increase of the distance from the working face to the observation station. The displacement characteristics of two sidewalls also decreased with the increase of the distance from the working face to the

observation station. Moreover, when the distance from the monitoring station to the working face exceeded 100.00 m, the roof to floor convergence and displacement of two sides became small. When the distance was 100.00 m, the roof to floor convergence and displacement of two sides started to grow linearly when approaching the working face, where roadway roof subsidence occurred with an obviously increased floor heaving. As the distance from the observation station to the working face decreased, the roof to floor convergence reached 1.08 m and the displacement of two sidewalls reached 1.16 m, which can seriously influence the regular mining operations. Therefore, it can be concluded that when the 2-2092 roadway advanced to the influencing scope of the adjacent goaf, the scope of the superposed

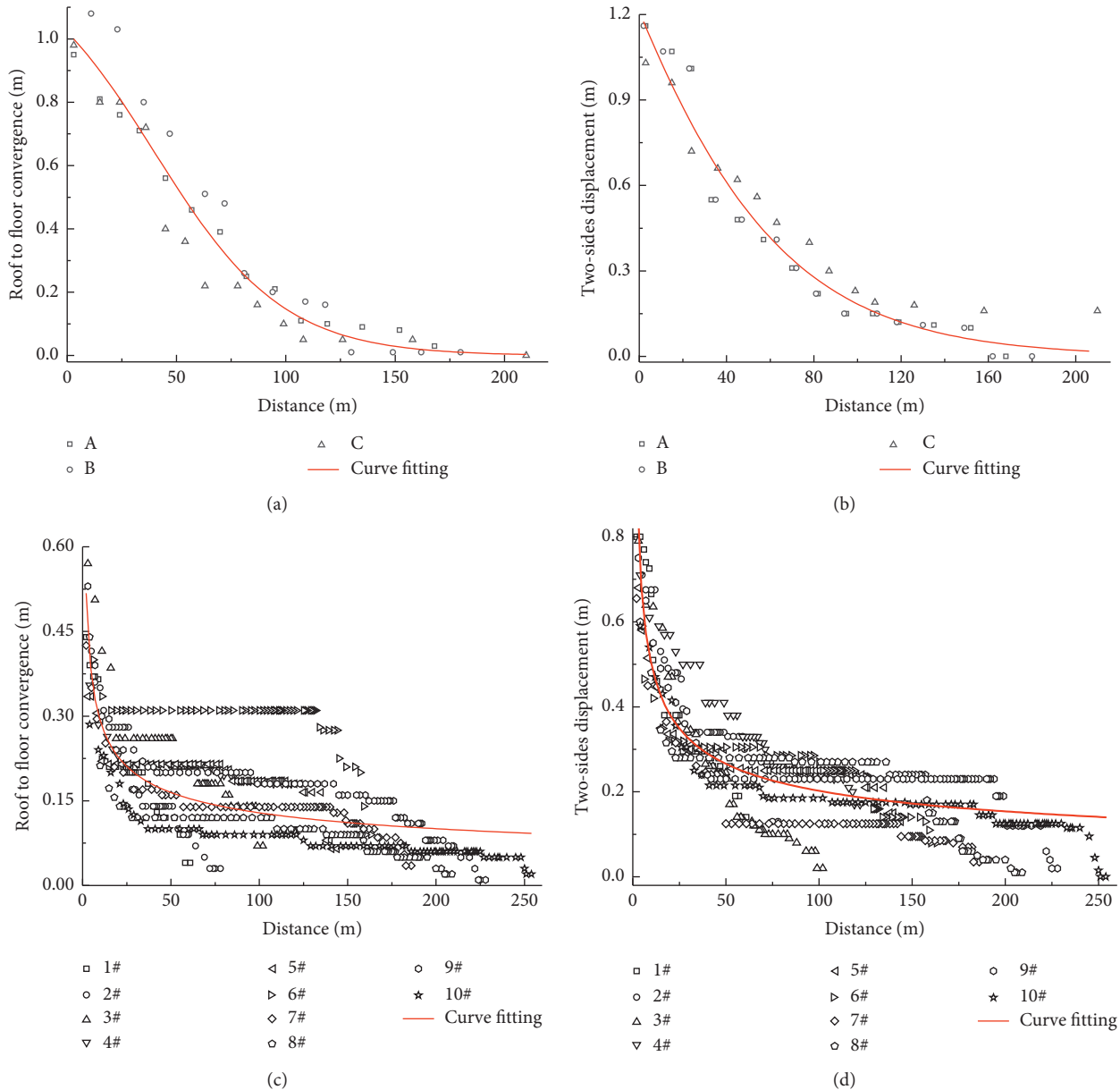


FIGURE 9: Comparison of roadway deformations in both fracturing area and nonfracturing area. (a) Results of the roof to floor convergence without fracturing. (b) Displacement of two sidewalls without fracturing. (c) Results of roof to floor convergence with fracturing. (d) Displacement of two sidewalls with fracturing.

influence of the mining-induced advanced abutment pressure would be approximately 100.00 m.

The monitoring results from 10 convergence monitoring stations arranged in the area with TDHT are shown in Figures 9(c) and 9(d). It can be shown that the roadway roof to floor convergence decreased as the distance from the working face to the observation station increased. Figure 9(d) showed that the displacement characteristics of two sidewalls also decreased with the longer distance. It could be known from Figures 9(c) and 9(d) that when the distance from the monitoring station to the working face exceeded 50.00 m within the fracturing area, the roof to floor convergence and displacement of two sidewalls were both

relatively small with little variations. When the distance from the monitoring station to the working face was 20.00–50.00 m, the roof to floor convergence and displacement of two sides increased. When the distance was smaller than 20.00 m, the maximum roof to floor convergence was 0.57 m and the maximum displacement of two sides was 0.79 m.

In fact, the large deformation is inevitable in some local regions such as the advanced abutment pressure influencing zone. The superposition, including local support strength decreasing, longer load-barring time, and unloading effect of coal seam, leads to the large deformation of the roadway. According to the monitoring data, the roof to floor



FIGURE 10: Roadway in the mining-induced advanced abutment pressure area of the fracturing area.

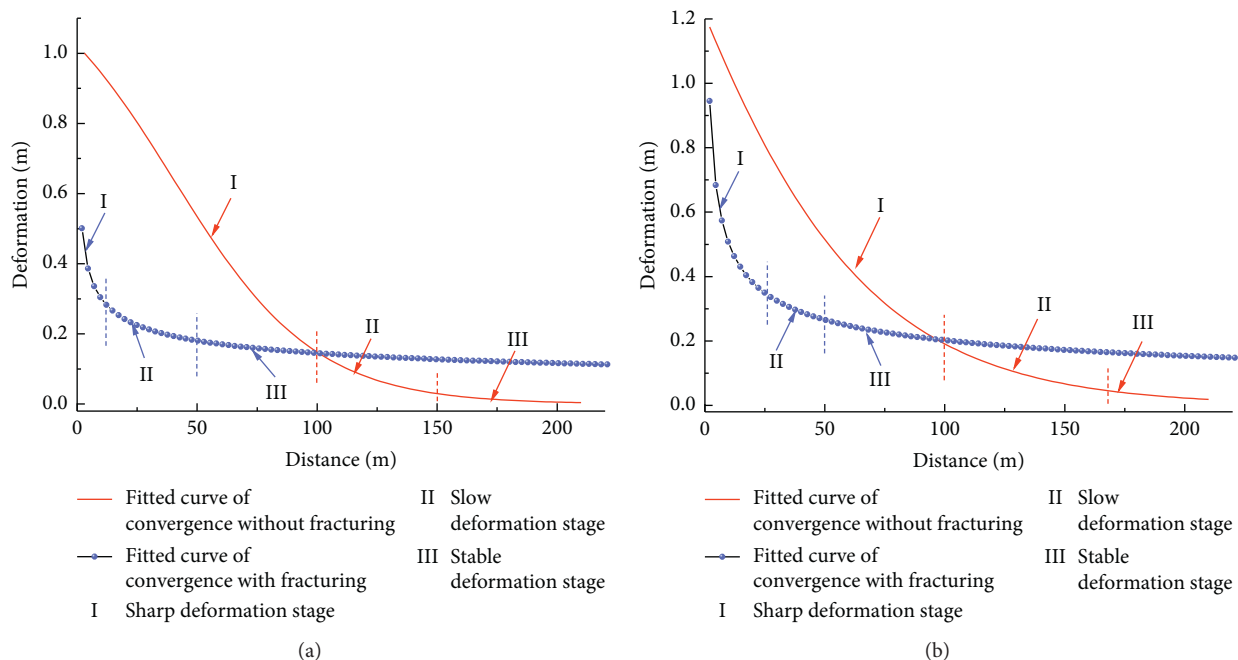


FIGURE 11: Comparison of fitted curves of the roadway deformations in the fracturing area and nonfracturing area. (a) Deformation results of the roof to floor convergence. (b) Deformation results of two sidewalls displacement.

convergence was reduced by over 47% and displacement of two sides reduced by over 31% in the area where the TDHT was adopted. The influencing scope of the superposed stress was reduced to 20.00–50.00 m with a reduction rate of 50–80%. Field observation suggested that the roadway experienced floor heaving but had no influence on single hydraulic props and equipment within the TDHT area, indicating that continuous production of the working face was achieved. The roadway site within the TDHT area is shown in Figures 10(a) and 10(b). Based on the above comparative analysis, the TDHT was found to effectively control the large deformation generated on the surrounding rocks of the deep roadway, which can reduce the cost of roadway maintenance and labour intensity.

5. Discussion

One side of the 2-2092 roadway in Ganhe coal mine was near the coal seam and the other side was close to the goaf of the

2-100 working face. According to the regular observation, the roadway deformation in the excavation period was smaller than the deformation before the 2-209 working face entered the influencing scope of the adjacent goaf and was smaller than the deformation when it entered the influencing scope of the goaf in the 2-100 working face. It could be seen that the deformation in the gob-side roadway had evident time and spatial effects, and the final large deformation of the roadway was caused by the superposition of both time and spatial effects.

From the stress analysis of the surrounding rocks in the 2-2092 roadway, the superposed stress-induced large deformation mainly consisted of the deep in situ stress, laterally transferred stress, and mining-induced advanced abutment pressure. Therefore, to better control the large deformation of the gob-side roadway, the TDHT can be adopted to alter the spatial structures formed in both the 2-209 working face goaf and adjacent goaf, which could lower the grades of laterally transferred stress and mining-induced

advanced abutment pressure, resulting in optimized stress environment and reduced deformation of the roadway. From Figures 9(a)–9(d), the fitted curves from the monitored data are given by

$$y = \frac{1.29}{1 + \exp[0.03 \times (x - 39.98)]},$$

$$y = \frac{3.95}{1 + \exp[0.02 \times (x + 37.73)]}, \quad (7)$$

$$y = 0.06x^{-0.32},$$

$$y = 1.24x^{-0.39},$$

where x indicates the distance of the monitoring station to the working face, m , and y indicates the deformation, m . Comparison of the fitted curves of the roadway deformations in the fracturing area and nonfracturing area is shown in Figure 11. It is dedicated that the fitted curves of roadway convergence could be divided into three stages, including sharp deformation stage (I), slow deformation stage (II), and stable deformation stage (III). It is also found that the obvious distance variation of the roadway decreased by 50%–80% from 100 m to 20–50 m, indicating that the scope of the mining-induced advanced abutment pressure in was greatly reduced the fracturing zone. In addition, the maximum roof to floor convergence and the maximum displacement of two sides reduced from 1.08 and 1.16 m to 0.57 and 0.95 m, respectively. By comparing Figures 11(a) and 11(b), it is dedicated that only three monitoring stations showed two-side large deformation appearing among the designed ten monitoring stations. It is suggested that the recording time of the roadway deformation would be set after a long stopping period, which could increase the roadway deformation. In general, the roadway deformation and influencing scope of the superposed stress were remarkably reduced and the stability of the roadway was effectively controlled.

The proposed TDHT for large deformation of the gob-side roadway can optimize the stress environment of the surrounding rocks in the roadway by adjusting the spatial structure of the overlying strata, which meets the goal of controlling the roadway deformation. Most of the existing control measures can exert a very good controlling effect on shallow roadway or roadway with low stress grade by controlling one side of the roadway (e.g., only gob side or front of the working face). However, for deep roadways or roadways with a high stress grade, it is necessary to control simultaneously the spatial structures at the overlying strata along both directions of the gob side.

6. Conclusions

- (1) Results from the continuous deformation observation in the 2-2092 roadway indicated that the large deformation of the gob-side roadway possessed evident time and spatial effects. The time effect was manifested by the fact that the roadway deformation

gradually increased during the excavation process. The spatial effect indicated that large deformation mainly took place in the gob-side roadway, and the roadway deformation was most severe within the scope of mining-induced advanced abutment pressure.

- (2) Based on the stress analysis of the 2-2092 roadway, it was found that the superposed stress mainly included the in situ stress in the area, laterally transferred stress formed in structures at overlying strata, and mining-induced advanced abutment pressure.
- (3) The proposed Two-Direction Hydrofracturing Technique could prevent further accumulation of large elastic energy at the overlying strata of the gob-side roadway by controlling the geometrical morphologies of the “cantilever beam” structure and “cantilever beam + hinged beam” structure formed at the overlying strata in the mining area.
- (4) The performance monitoring results indicated that, in the area applied with the two-direction hydrofracturing, the roof to floor convergence was reduced by over 47%, the displacement of two sidewalls was reduced by over 31%, and the influencing scope of mining-induced advanced abutment pressure declined to 20.00–50.00 m with a reduction of 50–80%, suggesting that the TDHT could provide an effective means of controlling the large deformation that is often found in the deep gob-side roadway.

Data Availability

The data used to support the findings of this study are included within the article.

Conflicts of Interest

The authors declare that they have no conflicts of interest.

Acknowledgments

This research was funded by Tiandi Science and Technology Co., Ltd., Science and Technology Innovation Venture Capital Special Project (Grant nos. 2019-TD-ZD008, 2020-TD-QN009, KJ-2018-TDKCZL-05, KJ-2019-TDKCQN-02, 2018-2-QN012, and 2019-TD-QN005).

References

- [1] British Petroleum, *BP Statistical Review of World Energy 2018*, British Petroleum, London, England, 2018.
- [2] H. P. Kang, G. Xu, B. M. Wang et al., “Forty years development and prospects of underground coal mining and strata control technologies in China,” *Journal of Mining and Strata Control Engineering*, vol. 1, no. 1, pp. 1–33, 2019.
- [3] China Coal Industry Association, *Annual Report on Coal Industry Development of 2018*, China Coal Industry Association, Beijing, China, 2019.
- [4] International Energy Agency IEA, *World Energy Outlook 2018*, International Energy Agency, IEA, Paris, France, 2019.

- [5] M. C. He, H. P. Xie, S. P. Peng, Y. D. Jiang et al., "Study on rock mechanics in deep mining engineering," *Chinese Journal of Rock Mechanics and Engineering*, vol. 24, no. 16, pp. 2803–2813, 2005.
- [6] N. Zhang, X. Y. Li, X. G. Zheng, and F. Xue, "The present situation and technical challenge of deep coal resources exploitation," in *Mining Technology of National Thousand-eter-eep Coal mines*, China University of Mining and Technology Press, pp.10–33, Xuzhou, China, 2013.
- [7] K. Zhang, Q. Wang, L. Chao et al., "Ground observation-based analysis of soil moisture spatiotemporal variability across a humid to semi-humid transitional zone in China," *Journal of Hydrology*, vol. 574, pp. 903–914, 2019.
- [8] J. W. Ye, W. J. Ju, X. Zhao et al., "Dynamic evolution characteristic on stope pressure in whole life cycle of stope," *Journal of China Coal Society*, vol. 44, no. 4, pp. 995–1002, 2019.
- [9] B. Shen, "Coal mine roadway stability in soft rock: a case study," *Rock Mechanics and Rock Engineering*, vol. 47, no. 6, pp. 2225–2238, 2014.
- [10] H. Lu, Y. Kang, L. Liu, and J. Li, "Comprehensive groundwater safety assessment under potential shale gas contamination based on integrated analysis of reliability-resilience-vulnerability and gas migration index," *Journal of Hydrology*, vol. 578, 2019.
- [11] H. Lu, P. Tian, and L. He, "Evaluating the global potential of aquifer thermal energy storage and determining the potential worldwide hotspots driven by socio-economic, geo-hydrologic and climatic conditions," *Renewable and Sustainable Energy Reviews*, vol. 112, pp. 788–796, 2019.
- [12] J. Zheng, W. Ju, X. Sun et al., "Analysis of hydro-fracturing technique using ultra-deep boreholes for coal mining with hard roofs: a case study," *Mining, Metallurgy & Exploration*, 2020.
- [13] K. Holub, J. Rušajová, and J. Holečko, "Particle velocity generated by rockburst during exploitation of the longwall and its impact on the workings," *International Journal of Rock Mechanics and Mining Sciences*, vol. 48, no. 6, pp. 942–949, 2011.
- [14] T. Zhou, J. B. Zhu, Y. Ju, and H. P. Xie, "Volumetric fracturing behaviour of 3D printed artificial rocks containing single and double 3D internal flaws under static uniaxial compression," *Engineering Fracture Mechanics*, vol. 205, pp. 190–204, 2019.
- [15] J. Qiu, X. Li, D. Li, Y. Zhao, C. Hu, and L. Liang, "Physical model test on the deformation behavior of an underground tunnel under blasting disturbance," *Rock Mechanics and Rock Engineering*, 2020.
- [16] B. H. G. Brady and E. T. Brown, *Rock Mechanics for Underground Mining*, Springer, London, England, 2006.
- [17] O. Pourhosseini and M. Shabanimashcool, "Development of an elasto-plastic constitutive model for intact rocks," *International Journal of Rock Mechanics and Mining Sciences*, vol. 66, no. 66, pp. 1–12, 2014.
- [18] X. F. Yu, "On the theory of axial variation and basic rules of deformation and fracture of rocks surrounding underground excavations," *Uranium Mining and Metallurgy*, vol. 1, no. 1, pp. 8–17, 1982.
- [19] C. M. Li, W. B. Shi, W. R. Liu, and R. M. Feng, "Elastic-plastic analysis of surrounding rock in deep roadway considering shear dilatancy property under non-uniform stress field," *Journal of Engineering Science and Technology Review*, vol. 10, no. 4, pp. 16–24, 2017.
- [20] M. Maleki and M. Mousivand, "Safety evaluation of shallow tunnel based on elastoplastic-viscoplastic analysis," *Scientia Iranica*, vol. 21, no. 5, pp. 1480–1491, 2013.
- [21] S. K. Sharan, "Analytical solutions for stresses and displacements around a circular opening in a generalized Hoek-Brown rock," *International Journal of Rock Mechanics and Mining Sciences*, vol. 45, no. 1, pp. 78–85, 2008.
- [22] D. Hou and X. Yang, "Physical modeling of displacement and failure monitoring of underground roadway in horizontal strata," *Advances in Civil Engineering*, vol. 2018, pp. 1–11, Article ID 2934302, 2018.
- [23] C. Q. Zhu, Z. Q. Yin, Z. Q. Yin, C. M. Li, and R. M. Feng, "Elastoplastic analysis of tunnel surrounding rocks based on the statistical damage constitutive model," *Journal of Engineering Science and Technology Review*, vol. 2016, no. 3, pp. 27–34, 2016.
- [24] W. Zheng, Q. Bu, and Y. Hu, "Plastic failure analysis of roadway floor surrounding rocks based on unified strength theory," *Advances in Civil Engineering*, vol. 2018, pp. 1–10, Article ID 7475698, 2018.
- [25] Y. Yuan, W. Wang, S. Li, and Y. Zhu, "Failure mechanism for surrounding rock of deep circular roadway in coal mine based on mining-induced plastic zone," *Advances in Civil Engineering*, vol. 2018, pp. 1–14, Article ID 1835381, 2018.
- [26] Y. Xue, F. Gao, X. Liu, and X. Liang, "Permeability and pressure distribution characteristics of the roadway surrounding rock in the damaged zone of an excavation," *International Journal of Mining Science and Technology*, vol. 27, no. 2, pp. 211–219, 2017.
- [27] Q. Sun, J. X. Zhang, Y. L. Huang et al., "Failure mechanism and deformation characteristics of gob-side entry retaining in solid backfill mining: a case study," *Natural Resources Research*, vol. 11, no. 1, pp. 1–13, 2019.
- [28] J. X. Zhang, H. Q. Jiang, X. X. Miao et al., "The rational width of the support body of gob-side entry in fully mechanized backfill mining," *Journal of Mining & Safety Engineering*, vol. 30, no. 2, pp. 159–164, 2013.
- [29] B. Mou, X. Li, Y. Bai, W. Liu, and H. Jing, "Finite element simulations of unequal-depth panel zones in steel beam-to-tubular column joints," *Journal of Constructional Steel Research*, vol. 162, 2019.
- [30] B. Mou, X. Li, Q. Qiao, B. He, and M. Wu, "Seismic behaviour of the corner joints of a frame under biaxial cyclic loading," *Engineering Structures*, vol. 196, 2019.
- [31] B. Mou, F. Zhao, Q. Y. Qiao et al., "Flexural behaviour of beam to column joints with or without an overlying concrete slab," *Engineering Structures*, vol. 199, 2019.
- [32] N. Zhang, L. Yuan, C. Han, J. Xue, and J. Kan, "Stability and deformation of surrounding rock in pillarless gob-side entry retaining," *Safety Science*, vol. 50, no. 4, pp. 593–599, 2012.
- [33] H. Kang, "Support technologies for deep and complex roadways in underground coal mines: a review," *International Journal of Coal Science & Technology*, vol. 1, no. 3, pp. 261–277, 2014.
- [34] C. Liu, X. Deng, J. Liu, T. Peng, S. Yang, and Z. Zheng, "Dynamic response of saddle membrane structure under hail impact," *Engineering Structures*, vol. 214, 2020.
- [35] C. Liu, F. Wang, X. Deng et al., "Hailstone-induced dynamic responses of pretensioned umbrella membrane structure," *Advances in Structural Engineering*, vol. 2020, Article ID 1369433220940149, 2020.
- [36] B. Mou and Y. Bai, "Experimental investigation on shear behavior of steel beam-to-CFST column connections with irregular panel zone," *Engineering Structures*, vol. 168, pp. 487–504, 2018.

- [37] B. Mou, Y. Bai, and V. Patel, "Post-local buckling failure of slender and over-design circular CFT columns with high-strength materials," *Engineering Structures*, vol. 210, 2020.
- [38] Y.-Q. Zhao, F.-L. He, and J.-K. Wu, "A new cable-truss structure for roadway driving next to goaf," *Geotechnical and Geological Engineering*, vol. 37, no. 1, pp. 389–400, 2019.
- [39] S. S. Peng and D. H. Y. Tang, "Roof bolting in underground mining: a state-of-the-art review," *International Journal of Mining Engineering*, vol. 2, no. 1, pp. 1–42, 1984.
- [40] J. W. Zheng, W. J. Ju, Z. Zhang et al., "Equivalent section supporting theory and its applications," *Journal of China Coal Society*, vol. 45, no. 3, pp. 1036–1043, 2020.
- [41] C.-L. Han, N. Zhang, B.-Y. Li, G.-Y. Si, and X.-G. Zheng, "Pressure relief and structure stability mechanism of hard roof for gob-side entry retaining," *Journal of Central South University*, vol. 22, no. 11, pp. 4445–4455, 2015.
- [42] Q. Ma, Y. L. Tan, Z. H. Zhao, Q. Xu, J. Wang, and K. Ding, "Roadside support schemes numerical simulation and field monitoring of gob-side entry retaining in soft floor and hard roof," *Arabian Journal of Geosciences*, vol. 11, p. 563, 2018.
- [43] B. X. Huang, S. L. Chen, and X. L. Zhao, "Hydraulic fracturing stress transfer methods to control the strong strata behaviours in gob-side gateroads of longwall mines," *Arabian Journal of Geosciences*, vol. 10, p. 236, 2017.
- [44] H. Kang, H. Lv, F. Gao, X. Meng, and Y. Feng, "Understanding mechanisms of destressing mining-induced stresses using hydraulic fracturing," *International Journal of Coal Geology*, vol. 196, pp. 19–28, 2018.
- [45] W. Yu, K. Li, and Z. Zhou, "Deformation mechanism and control technology of surrounding rock in the deep-buried large-span chamber," *Geofluids*, vol. 2020, pp. 1–22, Article ID 8881319, 2020.
- [46] W. Yu and F. Liu, "Stability of close chambers surrounding rock in deep and comprehensive control technology," *Advances in Civil Engineering*, vol. 2018, pp. 1–18, Article ID 6275941, 2018.
- [47] W. Yu, B. Pan, F. Zhang, S. Yao, and F. Liu, "Deformation characteristics and determination of optimum supporting time of alteration rock mass in deep mine," *KSCE Journal of Civil Engineering*, vol. 23, no. 11, pp. 4921–4932, 2019.
- [48] Z. Li, H. Zhou, D. Hu, and C. Zhang, "Yield criterion for rock like geomaterials based on strain energy and CMP model," *International Journal of Geomechanics*, vol. 20, no. 3, 2020.
- [49] H. P. Kang, G. F. Wang, P. F. Jiang et al., "Conception for strata control and intelligent mining technology in deep coal mines with depth more than 1 000 m," *Journal of China Coal Society*, vol. 43, no. 7, pp. 1789–1800, 2018.
- [50] Z. Ding, J. Jia, and R. Feng, "Effect of the vertical stress on CO₂ flow behavior and permeability variation in coalbed methane reservoirs," *Energy Science & Engineering*, vol. 7, no. 5, pp. 1937–1947, 2019.
- [51] F. Fraternali, I. Farina, and G. Carpentieri, "A discrete-to-continuum approach to the curvatures of membrane networks and parametric surfaces," *Mechanics Research Communications*, vol. 56, pp. 18–25, 2014.
- [52] M. Modano, F. Fabbrocino, A. Gesualdo, G. Matrone, I. Farina, and F. Fraternali, "On the forced vibration test by vibrodyne," in *5th ECCOMAS Thematic Conference on Computational Methods in Structural Dynamics and Earthquake Engineering*, Crete Island, Greece, May 2015.
- [53] F. Cui, T. H. Zhang, X. P. Lai, J. Cao, and P. Shen, "Study on the evolution law of overburden breaking angle under repeated mining and the application of roof pressure relief," *Energies*, vol. 12, no. 13, pp. 4513–4532, 2019.
- [54] Q. Liu, J. Chai, S. Chen, D. Zhang, Q. Yuan, and S. Wang, "Monitoring and correction of the stress in an anchor bolt based on pulse pre-pumped brillouin optical time domain analysis," *Energy Science & Engineering*, vol. 8, no. 6, pp. 2011–2023, 2020.
- [55] R. Barati and J. T. Liang, "A review of fracturing fluid systems used for hydraulic fracturing of oil and gas wells," *Journal of Applied Polymer Science*, vol. 131, no. 16, 2014.
- [56] R. J. Davies, S. A. Mathias, J. Moss, S. Hustoft, and L. Newport, "Hydraulic fractures: how far can they go?" *Marine and Petroleum Geology*, vol. 37, no. 1, pp. 1–6, 2012.
- [57] E. Detournay, "Mechanics of hydraulic fractures," *Annual Review of Fluid Mechanics*, vol. 48, no. 1, pp. 311–339, 2016.
- [58] P. Gupta and C. A. Duarte, "Simulation of non-planar three-dimensional hydraulic fracture propagation," *International Journal for Numerical and Analytical Methods in Geomechanics*, vol. 38, no. 13, pp. 1397–1430, 2014.